AIAA JOURNAL
Vol. 36, No. 7, July 1998

# Modeling Near-Wall Effects in Axially Rotating Pipe Flow by Elliptic Relaxation

B. A. Pettersson*
*Kongsberg Defence and Aerospace, N-3601 Kongsberg, Norway*
and
H. I. Andersson† and A. S. Brunvoll‡
*Norwegian University of Science and Technology, N-7034 Trondheim, Norway*

**The ability to faithfully reproduce the effect of axial rotation on fully developed turbulent pipe flow is investigated using a low-Reynolds-number, second-moment closure model. In particular, the impact of the pressure–strain model is scrutinized by adopting both linear and nonlinear models. Near-wall effects are modeled by elliptic relaxation, and model predictions are verified against direct numerical simulations as well as experimental results. The results suggest that pressure-strain models cubic in the Reynolds stresses seem unsuitable for this particular case, whereas the best overall performance is obtained by a model that retains terms quadratic in the Reynolds stress tensor. However, the stabilizing effect of the imposed axial rotation on the turbulence is in general overpredicted by the models.**

## Nomenclature

$A$ = anisotropy parameter, $1 - \frac{9}{8}(A_2 - A_3)$
$A_2$ = second Reynolds stress invariant, $a_{ij}a_{ij}$
$A_3$ = third Reynolds stress invariant, $a_{ik}a_{kj}a_{ji}$
$a_{ij}$ = Reynolds stress anisotropy, $\overline{u_iu_j}/k - 2\delta_{ij}/3$
$C_{ij}$ = convective transport of $\overline{u_iu_j}$
$d^p_{ij}$ = pressure diffusion of $\overline{u_iu_j}$
$d^t_{ij}$ = turbulent diffusion of $\overline{u_iu_j}$
$d^v_{ij}$ = viscous diffusion of $\overline{u_iu_j}$
$f_{ij}$ = intermediate variable, $\wp_{ij}/k$
$k$ = turbulent kinetic energy, $\frac{1}{2}\overline{u_iu_i}$
$L$ = characteristic turbulent length scale
$N$ = rotation number, $U_{\theta,\text{wall}}/U_b$
$P$ = mean pressure
$P_{ij}$ = shear generation of $\overline{u_iu_j}$
$p$ = fluctuating pressure
$R$ = pipe radius
$Re$ = Reynolds number, $2RU_b/\nu$
$Re_*$ = Reynolds number, $2Ru_*/\nu$
$r$ = radial direction defined in Fig. 1
$S_{ij}$ = mean rate of strain, $\frac{1}{2}(\partial U_i/\partial x_j + \partial U_j/\partial x_i)$
$T$ = characteristic turbulent timescale
$U_b$ = mean bulk velocity
$U_i$ = mean velocity component in $x_i$ direction
$U_{\theta,\text{wall}}$ = circumferential wall velocity
$u_i$ = velocity fluctuation in $x_i$ direction
$u_*$ = wall friction velocity, $\sqrt{(\tau_w/\rho)}$
$\overline{u_iu_j}$ = kinematic Reynolds stress
$x_i$ = spatial coordinate, $(x_1, x_2, x_3) = (r, \theta, z)$
$y$ = distance measured from the wall
$y^+$ = inner variable, $u_*y/\nu$
$z$ = axial direction defined in Fig. 1
$\delta_{ij}$ = Kronecker delta
$\varepsilon$ = energy dissipation rate, $\frac{1}{2}\varepsilon_{ii}$
$\hat{\varepsilon}$ = modified dissipation rate, $\sqrt{(\varepsilon^2 + \Phi^2)}$
$\varepsilon_{ij}$ = dissipation rate tensor
$\theta$ = circumferential direction defined in Fig. 1
$\lambda$ = friction factor, $8(u_*/U_b)^2$
$\mu$ = dynamic viscosity
$\nu$ = kinematic viscosity
$\rho$ = density
$\tau_w$ = wall shear stress in axial direction, $\mu\, \mathrm{d}U_z/\mathrm{d}r$
$\phi_{ij}$ = pressure–strain interactions
$\Phi$ = mean viscous dissipation function, $2\nu S_{ij}S_{ij}$
$\wp_{ij}$ = relaxed pressure–strain tensor

Received Sept. 12, 1997; revision received March 9, 1998; accepted for publication March 17, 1998. 

*Project Engineer, New Anti-Ship Missile Program.
†Professor, Faculty of Mechanical Engineering, Division of Applied Mechanics.
‡Graduate Student, Division of Applied Mechanics.

## Introduction

TURBULENT flows affected by centrifugal and Coriolis forces are frequently encountered in engineering applications as well as in nature. These body forces are known to considerably alter the mean flowfield and the intensity and structure of the turbulence. Because the engineering approach to fluid flow calculations is based on the Reynolds-averaged Navier–Stokes equations, the success of any computational fluid dynamics analysis relies heavily on the turbulence model embodied in the actual computer code. It is therefore unfortunate that the widely used $k$-$\varepsilon$ model, like any other turbulence model that utilizes Boussinesq's linear stress–strain relationship, is unable to naturally account for these effects. The effects of centrifugal and Coriolis forces are, on the other hand, automatically accounted for within the framework of second-moment closure (SMC) modeling, which is based on the exact transport equations governing the individual Reynolds-stress components.

Turbulent flow inside an axially rotating pipe not only is of theoretical interest but also has some direct practical applications, e.g., the internal cooling in turbomachinery. Another very interesting feature of this particular flowfield is the analogies with three-dimensional boundary layers, which are of considerable practical importance in industry. Kikuyama et al.[1] studied experimentally the flow in the entry region of a rotating pipe, and Yoo et al.[2] predicted this flow with a number of different closure models, including two near-wall SMC models. Yoo et al.[2] concluded that closures that take into account the anisotropy of the turbulence are required to faithfully predict this particular flow and, moreover, that the turbulence near the wall is not in equilibrium. The latter observation consequently implies that the commonly used wall-function approach should be abandoned. In spite of the simple geometry, the developing flow is three dimensional and rather complex and thus provides a severe test for any turbulence closure.

Murakami and Kikuyama,[3] Kikuyama et al.,[4] Reich and Beer,[5] and Imao et al.[6] studied experimentally the effect of axial rotation on fully developed turbulent pipe flow. Hirai et al.[7] employed three different turbulence models: two based on the eddy-viscosity hypothesis and one full SMC model. Although their numerical computations used the wall-function approach, they reached the same conclusion

as Yoo et al.,[2] namely, that an anisotropic closure model is required. This flow has more recently been calculated by Shih et al.[8] and Wallin and Johansson[9] using algebraic Reynolds-stress models (ARSM) with a cubic nonlinearity, whereas Malin and Younis[10] and Speziale et al.[11] used full SMCs with both linear and nonlinear pressure–strain models. In the latter studies, wall functions were used to bridge the semiviscous sublayer adjacent to the wall.[10,11] Malin and Younis[10] noted, however, that "the wall-function approach becomes unsuitable at high rotation rates, as near-wall viscous effects become pervasive due to the fact that the flow, being subjected to large wall rotation, changes its direction very rapidly in the thin near-wall layer." Moreover, because the mean circumferential (swirl) velocity is generated by the secondary Reynolds shear stress $\overline{u_r u_\theta}$, the model calculations by Speziale et al.[11] demonstrated that "the generation of a non-zero mean swirl velocity is largely a near-wall effect at high Reynolds numbers." For certain parameter combinations (rotation and Reynolds numbers), the turbulent flow in an axially rotating pipe can be satisfactorily described with a suitable closure in combination with the wall-function approach. For general applicability, however, a low-Reynolds-number model should be employed so that boundary conditions are imposed at the wall itself rather than at a wall-adjacent computational node.

An outstanding feature of the fully developed case as compared with the entry flow is that the mean flowfield can be considered as one dimensional and two componential. The set of governing equations thus reduces to a set of ordinary differential equations (ODEs) that can be solved numerically to practically any degree of accuracy, and the true performance of the closure model is revealed. In contrast to its laminar counterpart, the mean axial velocity component in turbulent pipe flow is dependent on the imposed axial rotation. Furthermore, the centrifugal force caused by the superimposed circumferential velocity has a stabilizing effect on the turbulence across the entire pipe, and the turbulent momentum transfer is therefore strongly suppressed. The present study focuses on the assessment of a near-wall model developed by Durbin.[12] This SMC model has recently proven successful in predicting unidirectional mean flows subjected to system rotation[13] and streamline curvature.[14] The performance of this state-of-the-art model is explored in fully developed pipe flow subjected to constant axial rotation.

Substantial advances in SMC modeling have been made in recent years, notably the evolution of closure models free of wall distances and wall normals. This particular feature makes these models applicable to flows with geometrically complex boundaries. The very important pressure–strain interaction term is the focus of much of the research efforts at this closure level, especially its mean-strain contribution. The objective of the present study is to investigate whether nonlinear pressure–strain models, used in conjunction with the relaxation approach[12] to model near-wall effects, can improve the predictions as compared with a pressure–strain model that is linear in the Reynolds stresses. Model predictions will be verified against recent experimental results reported by Imao et al.[6] and direct numerical simulation (DNS) data.[15,16]

## Mathematical Model

Consider fully developed turbulent pipe flow subjected to axial rotation (Fig. 1). The mean flowfield is assumed to be one dimensional and two componential so that the two nonzero mean velocity components $\boldsymbol{U} = \{0, U_\theta(r), U_z(r)\}$ are homogeneous in the axial $z$ and circumferential $\theta$ directions. The equations governing the mean momentum can be written as

$$0 = -\frac{\partial P}{\partial z} + \mu\left(\frac{\mathrm{d}^2 U_z}{\mathrm{d}r^2} + \frac{1}{r}\frac{\mathrm{d}U_z}{\mathrm{d}r}\right) - \frac{1}{r}\frac{\mathrm{d}}{\mathrm{d}r}(r\rho\overline{u_r u_z}) \tag{1}$$

$$0 = \mu\left(\frac{\mathrm{d}^2 U_\theta}{\mathrm{d}r^2} + \frac{1}{r}\frac{\mathrm{d}U_\theta}{\mathrm{d}r} - \frac{U_\theta}{r^2}\right) - \frac{1}{r^2}\frac{\mathrm{d}}{\mathrm{d}r}(r^2\rho\overline{u_r u_\theta}) \tag{2}$$

for a constant property fluid in a cylindrical coordinate system. Here, the mean pressure $P = P(r, z)$ decreases linearly in the axial direction such that $\partial P/\partial z$ is a negative constant. The a priori unknown Reynolds shear stresses, $-\rho\overline{u_r u_z}$ and $-\rho\overline{u_r u_\theta}$, can be obtained from the transport equation governing the kinematic Reynolds-stress tensor $-\overline{u_i u_j}$, which can be written as

$$\overbrace{U_k\frac{\partial\overline{u_i u_j}}{\partial x_k}}^{C_{ij}} = \overbrace{-\left(\overline{u_i u_k}\frac{\partial U_j}{\partial x_k} + \overline{u_j u_k}\frac{\partial U_i}{\partial x_k}\right)}^{P_{ij}} + \overbrace{\mu\frac{\partial^2\overline{u_i u_j}}{\partial x_k\partial x_k}}^{d^v_{ij}}$$
$$\overbrace{-\frac{\partial}{\partial x_k}\left(\overline{u_i u_j u_k} + \frac{\overline{pu_i}}{\rho}\delta_{jk} + \frac{\overline{pu_j}}{\rho}\delta_{ik}\right)}^{d^t_{ij}+d^p_{ij}} + \wp_{ij} - \frac{\overline{u_i u_j}}{k}\varepsilon \tag{3}$$

where the relaxed pressure–strain tensor is defined as

$$\wp_{ij} = \underbrace{\overline{\frac{p}{\rho}\left(\frac{\partial u_i}{\partial x_j} + \frac{\partial u_j}{\partial x_i}\right)}}_{\phi_{ij}} - \varepsilon_{ij} + \frac{\overline{u_i u_j}}{k}\varepsilon \tag{4}$$

in Cartesian tensor notation.

Turbulent diffusion is modeled by gradient diffusion as

$$d^t_{ij} = \frac{\partial}{\partial x_p}\left(C_K\overline{u_p u_m}T\frac{\partial\overline{u_i u_j}}{\partial x_m}\right) \tag{5}$$

whereas the pressure-diffusion term is modeled as

$$d^p_{ij} = -C^*_K\frac{\partial}{\partial x_m}\left[(\overline{u_i u_n}\delta_{jm} + \overline{u_j u_n}\delta_{im})T\frac{\partial k}{\partial x_n}\right] \tag{6}$$

following Fu.[17] However, because the pressure-diffusion term originally was intended for isotropic turbulence, the coefficient $C^*_K = 0.4AC_K$ is made a function of the stress anisotropy parameter $A$. The objective for adopting Eq. (6) is to decrease the turbulent timescale $k/\varepsilon$ to reduce the turbulent kinetic energy level in the pipe core, which otherwise is substantially overpredicted. The timescale $T$ is taken as[12] $T = \max[k/\varepsilon, 6\sqrt{(\nu/\varepsilon)}]$. The dissipation-rate tensor is assumed to be isotropic in the limit of homogeneous turbulence, i.e., $\varepsilon_{ij} = \frac{2}{3}\delta_{ij}\varepsilon$, and the relaxed pressure–strain tensor takes its homogeneous form $\wp^h_{ij} = \phi_{ij} + \varepsilon a_{ij}$. Nonlocal effects on $\wp_{ij}$, associated with the proximity of a solid boundary, are modeled by elliptic relaxation[12]:

$$L^2\nabla^2 f_{ij} - f_{ij} = -\wp^h_{ij}/k \tag{7}$$

where $f_{ij} = \wp_{ij}/k$ and $L = C_L\max[k^{3/2}/\varepsilon, C_\eta(\nu^3/\varepsilon)^{1/4}]$. The present study adopts a somewhat modified form[13] of the turbulent length scale when the relaxation equation is used in conjunction with nonlinear pressure–strain models, i.e., $L = \tilde{C}_L\max[k^{3/2}/\varepsilon, \tilde{C}_\eta(\nu^3/\hat{\varepsilon})^{1/4}]$, where the coefficients $\tilde{C}_L = C_L A_2^{1/2}$ and $\tilde{C}_\eta = C_\eta A_2^{-1/2}\exp\{-[(1+A_3)/(0.1+A_2)]^2\}$ have been made functions of the second $A_2$ and third $A_3$ Reynolds-stress invariants. To prevent excessive values of $L$ close to a solid boundary if the flow is relaminarized,[13] the scalar dissipation rate in Kolmogorov's length scale was furthermore replaced by $\hat{\varepsilon} = (\varepsilon^2 + \Phi^2)^{1/2}$, where $\Phi = 2\nu S_{ij}S_{ij}$ is the mean viscous dissipation function. In the nonrotating case $N = 0$, the dimensionless dissipation rate $\varepsilon^+ \equiv \varepsilon\nu/u_*^4$ equals $\varepsilon/\Phi$ at the pipe wall. Because $\varepsilon^+$ is about 0.25 in turbulent pipe flow (cf. Ref. 15), the modified dissipation rate $\hat{\varepsilon}$ becomes substantially greater than $\varepsilon$ in the immediate vicinity of the wall. However, the subsequent reduction of

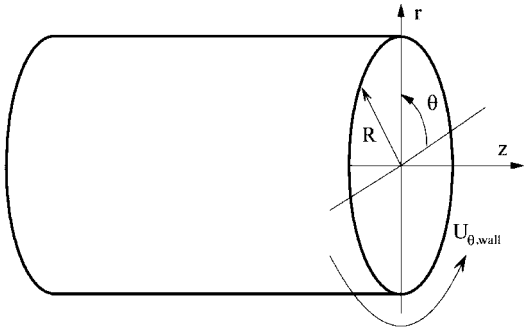


**Fig. 1 Schematic of flow configuration.**

**Table 1 Model constants**

| Model | $C_{\varepsilon 1}$ | $C_{\varepsilon 2}$ | $C_\varepsilon$ | $C_K$ | $C_L$ | $C_\eta$ |
|---|---|---|---|---|---|---|
| IP | 1.44 | 1.90 | 0.14 | 0.19 | 0.20 | 80.0 |
| SSG | 1.40 | 1.83 | 0.19 | 0.21 | 0.21 | 424 |
| RLA | 1.44 | 1.85 | 0.14 | 0.19 | 0.18 | 647 |
| FLT | 1.44 | 1.85 | 0.19 | 0.21 | 0.33 | 700 |

Kolmogorov's length scale close to the solid boundary is compensated by numerically increasing the product $\tilde{C}_L\tilde{C}_\eta$. As discussed by Pettersson and Andersson,[13] the replacement of $\varepsilon$ by $\hat{\varepsilon}$ purposely affects the predictions.

The present study adopts four different models for the pressure–strain tensor $\phi_{ij}$: 1) the linear isotropization-of-production model in which the convective transport $C_{ij}$ is included (for example, Ref. 14); 2) the model by Speziale et al.,[18] which is quadratic in the Reynolds-stress tensor; and, finally, the two cubic models by 3) Ristorcelli et al.[19] and 4) Fu et al.[20] These are hereafter denoted IP, SSG, RLA, and FLT, respectively. Inclusion of the convective transport $C_{ij}$ in the IP model is believed to be important in predictions of flows severely affected by streamline curvature or system rotation. Note that the inclusion of $C_{ij}$ does not alter the frame indifferent property of the original IP model and is therefore not strictly needed to attain an objective model. Nevertheless, inclusion of $C_{ij}$ seems in general to improve predictions, and considerable improvements were indeed observed by Pettersson et al.[14] for a Couette flow case. The SSG model has proven to outperform the linear IP model for a variety of flows and performs equivalently to the RLA model, at least for simple planar flows.[19] The RLA model has the same tensorial basis as the FLT model but employs variable coefficients that are functions of the Reynolds-stress invariants. A particularly interesting feature of the RLA model is that it is consistent with the principle of material frame indifference in the limit of two-componential turbulence and thus represents a more general class of pressure–strain models.

The dissipation rate of turbulent kinetic energy is obtained from its own modeled transport equation

$$\frac{\mathrm{D}\varepsilon}{\mathrm{D}t} = \frac{1}{T}\left[C_{\varepsilon 1}\left(1 + 0.1\frac{P_{kk}}{2\varepsilon}\right)\frac{P_{kk}}{2} - C_{\varepsilon 2}\varepsilon\right] + \frac{1}{2}\left(d^v_{kk} + \frac{C_\varepsilon}{C_K}d^t_{kk}\right) \tag{8}$$

which is solved coupled with the model equation governing the turbulent kinetic energy

$$\frac{\mathrm{D}k}{\mathrm{D}t} = \frac{P_{kk}}{2} - \varepsilon + \frac{1}{2}\left(d^v_{kk} + d^t_{kk} + d^p_{kk}\right) \tag{9}$$

Pressure diffusion is not accounted for in the dissipation-rate equation (8). Model constants are listed in Table 1.

## Numerical Approach

A particularly attractive feature of this model problem is that, within the framework of transport modeling, the set of governing equations reduces to a set of ODEs that can be solved numerically to practically any degree of accuracy. The governing set of equations consists of two equations for the mean flow, five equations for the Reynolds stresses ($\overline{u_r^2}$, $\overline{u_z^2}$, $\overline{u_r u_z}$, $\overline{u_r u_\theta}$, and $\overline{u_\theta u_z}$), together with their corresponding relaxation equations, and the turbulent kinetic energy and dissipation rate equations. The circumferential normal stress component is subsequently obtained from the relation $\overline{u_\theta^2} = 2k - \overline{u_r^2} - \overline{u_z^2}$. The resulting set of difference equations is solved semi-implicitly as coupled $k$-$\varepsilon$ and $\overline{u_i u_j}$-$f_{ij}$ systems by a pseudo-time-marching scheme until a steady-state solution is reached. Spatial derivatives are replaced by second-order-accurate, central-difference approximations. No-slip boundary conditions were used at the solid walls together with $k = \mathrm{d}k/\mathrm{d}r = 0$ for the $k$-$\varepsilon$ system and $f_{ij} = -20\nu^2(\overline{u_i u_j})_1/(\varepsilon_{\text{wall}} y_1^4)$ if $i$ and/or $j$ is in the wall-normal direction, $f_{ij} = 0$ else. Subscript 1 denotes the wall-adjacent computational node, and $y$ is the distance measured from the wall. The boundary condition for $f_{ij}$ is derived from the local solution of the model equation governing the wall-normal stress component ($\overline{u_r^2}$) at the wall.[12] It can readily be seen that the two wall boundary conditions for $k$ are formally equivalent with using $k = 0$ and $\varepsilon = 2\nu k_1/y_1^2$. Typically 100 grid points were nonuniformly distributed from the wall to the axis of the pipe such that the first computational node was situated at $y^+ \approx 0.5$. Grid independence was verified by using twice as many grid points without any discernible effect on the results. The solution was assumed to have reached a steady state when the sum of absolute normalized residuals across the pipe, normalized with the time step, fell below $10^{-5}$.

## Results

Model predictions are compared with DNS data[15,16] at $Re_* = 3.6 \times 10^2$, which corresponds to $Re \approx 5.3 \times 10^3$, and rotation numbers $N = 0$, 0.32, and 0.61. To examine the effect of the Reynolds number, comparisons are also made with the experimental results recently reported by Imao et al.[6] at $Re = 2 \times 10^4$ and $N = 0$ and 0.5. For some parameter combinations, however, the calculations unfortunately failed to converge; cf. Table 2.

### Mean Flow Quantities

The predicted mean-velocity distributions are compared with DNS data and experimental results in Figs. 2 and 3. The mean axial velocity profile is deformed to become more laminarlike due to the axial rotation. The centerline velocity $U_z(r = 0)$ in Fig. 2 increases with rotation number, whereas a reduction can be observed near the wall. Figure 3 displays the mean circumferential velocity, and both the DNS data and experimental results indicate a nearly parabolic distribution, i.e., $U_\theta \propto r^n$, where $n \approx 2$, except close to the wall, where the DNS results exhibit an almost linear variation ($n \approx 1$). The best overall performance is achieved by the SSG model, especially concerning the $U_\theta$ component. It is noteworthy that both cubic models (RLA and FLT) failed to converge at the highest Reynolds number and the former even at the lowest Reynolds number in the case of $N = 0.61$. These results are therefore not presented in the figures. This surprising failure can be illustrated by the RLA results in Fig. 3a at $N = 0.32$, where the predicted $U_\theta$ distribution displays the opposite trend as compared with the DNS data; i.e., $\mathrm{d}^2U_\theta/\mathrm{d}r^2$ becomes negative rather than positive. Although the FLT model produces the best predictions of the axial mean-velocity component in Fig. 2a, the circumferential component in Fig. 3a exhibits a nearly linear variation similar to that obtained with the simple IP model. Recall that a strictly linear $U_\theta$ profile corresponds to solid body rotation, i.e., the laminar solution and the solution obtained with closure models based on Boussinseq's linear stress–strain relationship (e.g., see Ref. 7).

The centrifugal force caused by the imposed rotation of the pipe has a stabilizing effect on the turbulence. Because the friction velocity is kept constant in the computations at $Re_* = 3.6 \times 10^2$, it is expected that the mean bulk velocity should change with the rate of rotation. At $Re = 2 \times 10^4$, however, the mean bulk velocity is held constant in the computations, and this implies that the friction velocity is expected to vary. The stabilizing effect of axial rotation on fully developed turbulent pipe flow is summarized in Table 2, where the friction factor $\lambda = 8(u_*/U_b)^2$ is presented for different rotation numbers. All models, except RLA, are able to capture the reduction of $\lambda$ with increasing pipe rotation. Both the IP and SSG models, however, significantly overpredict this stabilizing effect. The exaggerated reduction of the wall friction is fully consistent with the predictions by Malin and Younis.[10] Attempts were also made to compute the case $Re = 2 \times 10^4$ and $N = 1.0$. However, the stabilizing influence of the rotation completely quenched the turbulence, and the laminar solution was returned in contrast to the experiments by Imao et al.[6] in which turbulence still prevailed.

**Table 2 Friction factor ratio $\lambda_{N=0}/\lambda$**

| $N$ | DNS[16] | Reference 6 | IP | SSG | FLT | RLA |
|---|---|---|---|---|---|---|
| 0.32 | 1.11 | ND | 1.16 | 1.18 | 1.04 | 1.05 |
| 0.61 | 1.22 | ND | 1.58 | 1.64 | 1.20 | NC |
| 0.50 | ND[a] | 1.20 | 1.30 | 1.33 | NC[b] | NC |

[a]ND: no data available.
[b]NC: no convergence achieved.

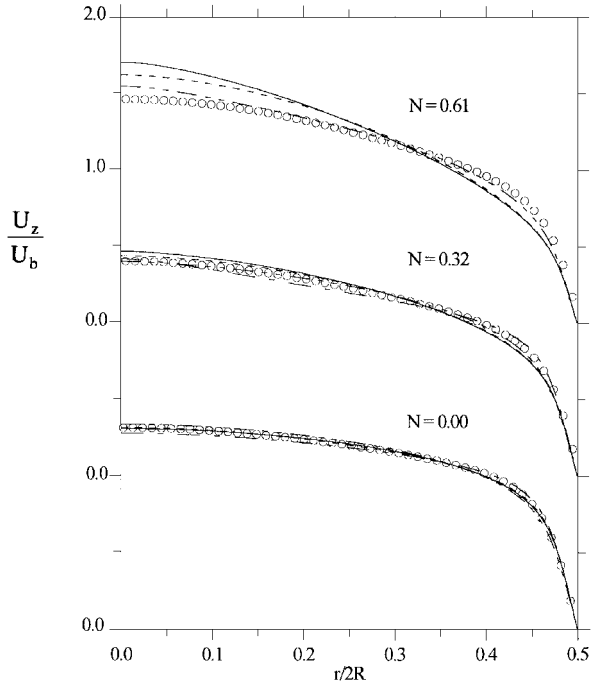


a) $Re \approx 5.3 \times 10^3$

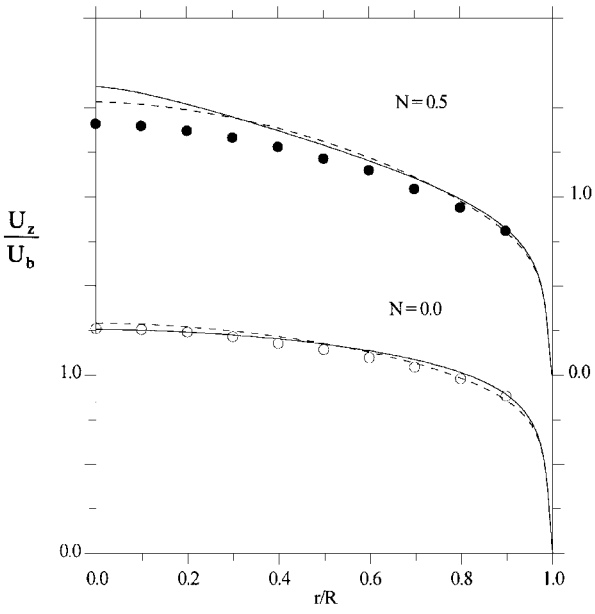


b) $Re = 2 \times 10^4$

**Fig. 2 Mean axial velocity: ○, DNS[15,16]; ●, experiments[6]; ——, IP; - - - -, SSG; - - - -, FLT; and — - —, RLA.**

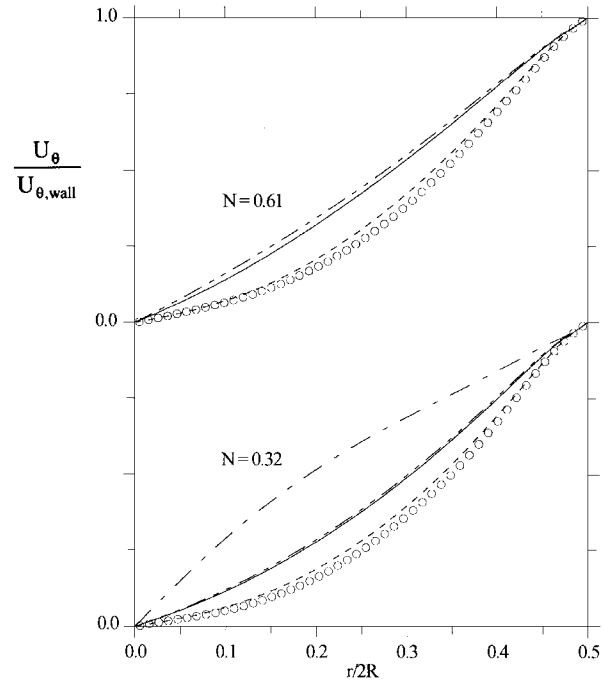


a) $Re \approx 5.3 \times 10^3$

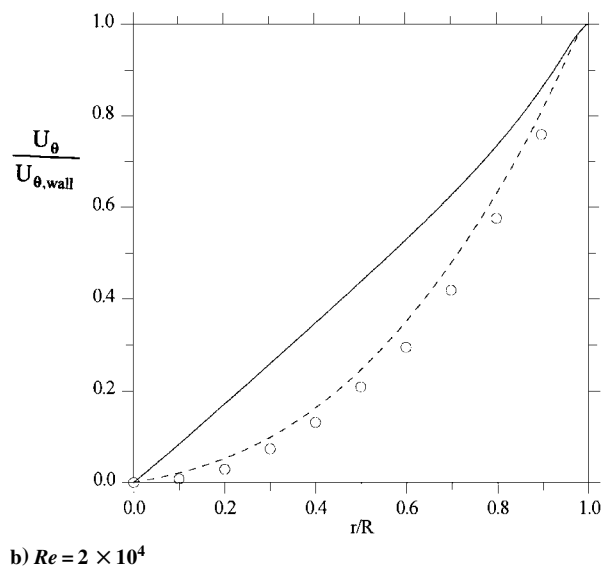


b) $Re = 2 \times 10^4$

**Fig. 3 Mean circumferential velocity. Legends as in Fig. 2.**

**Turbulence Quantities**

In the present study, all components of the Reynolds-stress tensor are nonzero due to the imposed pipe rotation, whereas the $\overline{u_r u_\theta}$ and $\overline{u_z u_\theta}$ components are zero in a fixed pipe. The mean flowfield is strongly coupled with the off-diagonal components $\overline{u_r u_\theta}$ and $\overline{u_r u_z}$; cf. Eqs. (1) and (2). For instance, rearrangement of Eq. (2) and subsequent integration gives

$$\nu \frac{\mathrm{d}}{\mathrm{d}r}\left(\frac{U_\theta}{r}\right) = \frac{\overline{u_r u_\theta}}{r} \tag{10}$$

which shows that solid body rotation is achieved in the absence of $\overline{u_r u_\theta}$. The predicted shear-stress components are compared with the DNS data in Fig. 4. Note that the level of $\overline{u_r u_\theta}$ is roughly one decade below that of the two other shear-stress components, but $\overline{u_r u_\theta}$ is nevertheless essential in the determination of $U_\theta$. The $\overline{u_r u_\theta}$ component is best predicted by the SSG model, i.e., in accordance with the excellent results in Fig. 3, whereas the IP and FLT models underpredict the peak close to the wall and consequently also the slope in the pipe core. The anomalous prediction of $U_\theta$ obtained with the RLA model can now be explained by the results in Fig. 4a at $N = 0.32$. Because the model returns a negative $\overline{u_r u_\theta}$ component, an opposite effect of the turbulence on the circumferential mean-velocity component is to be expected; i.e., the turbulence tends to increase the mean velocity as compared with the laminar solution instead of reducing it. A possible explanation of this erroneous behavior will be given in the Discussion. Moreover, the right-hand side of Eq. (10) is substantially reduced near the pipe wall, thereby explaining the almost linear variation of $U_\theta$ in the near-wall region (see Fig. 3a) obtained with all models.

In the nonrotating pipe ($N = 0$), $\overline{u_r u_z}$ is the only nonzero off-diagonal component of the Reynolds-stress tensor, and this component alone determines the $U_z$ profile; cf. Eq. (1). In accordance with the predicted axial mean velocity in Fig. 2a, the predicted distribution of $\overline{u_r u_z}$ obtained by the FLT model (Fig. 4b) is in closest correspondence with the DNS data, especially at the highest rotation number. Because all models predict $\overline{u_z u_\theta} < 0$, as shown in Fig. 4c, the presence of the term $2\overline{u_z u_\theta} U_\theta / r$ in the $\overline{u_r u_z}$ transport equation causes a reduction of the $\overline{u_r u_z}$ component when the pipe is rotated

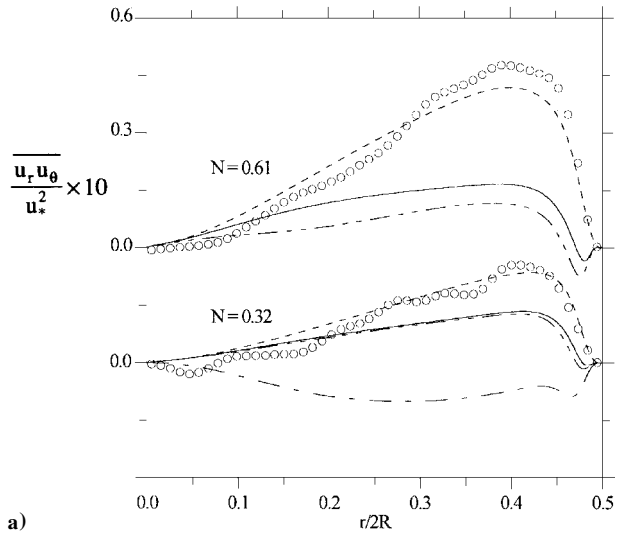


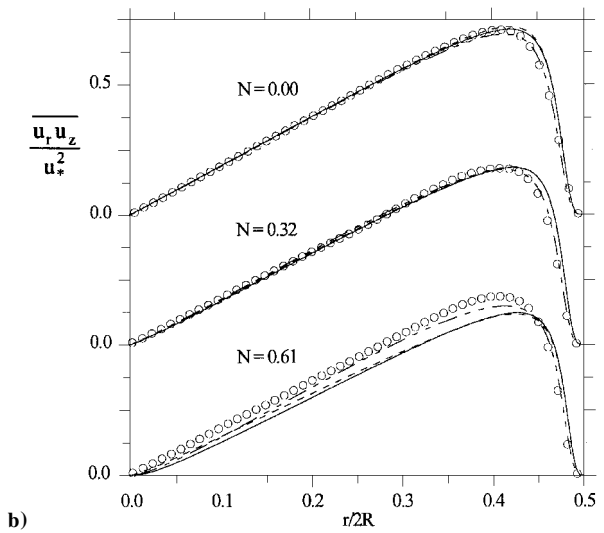


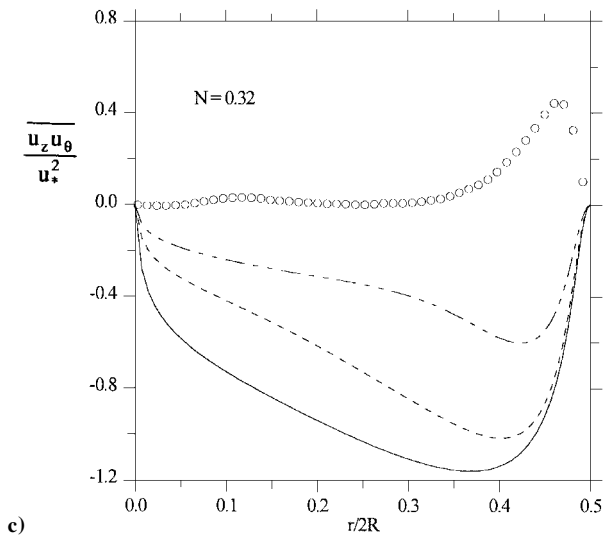


**Fig. 4 Turbulent shear stresses. Legends as in Fig. 2.**

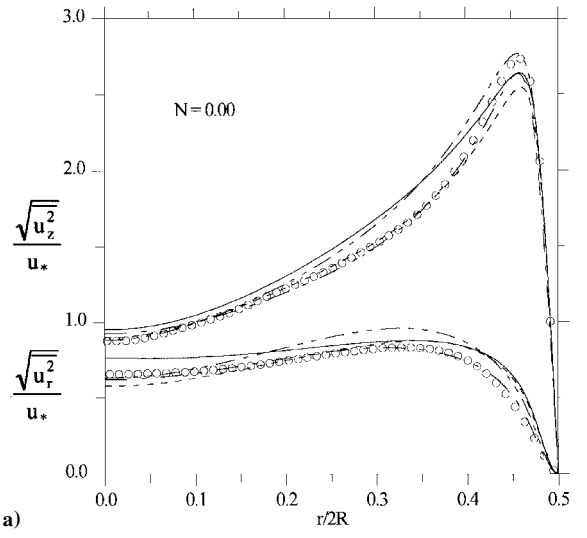


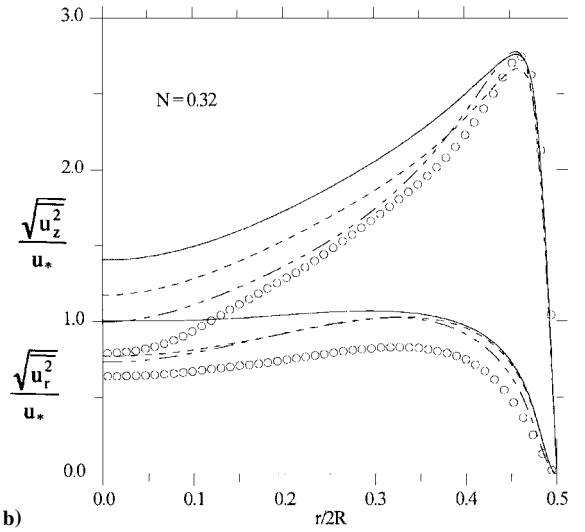


**Fig. 5 Axial and radial rms distribution. Legends as in Fig. 2.**

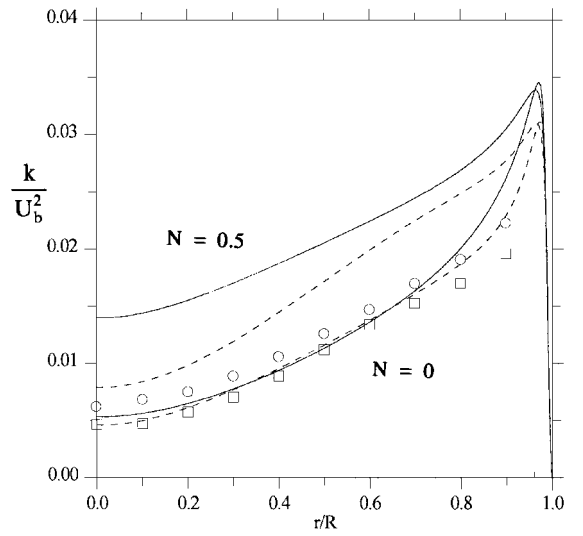


**Fig. 6 Turbulent kinetic energy at $Re = 2 \times 10^4$: symbols, experiments[6]; ——, IP; - - - -, SSG; ○, $N = 0.0$; and □, $N = 0.5$.**

and, consequently, a more laminarlike mean axial velocity profile. However, because the FLT model returns the lowest level of the $\overline{u_z u_\theta}$ component, less reduction of the $\overline{u_r u_z}$ stress can be expected. A similar trend is also observed at the highest rotation number (not shown here). The striking difference between the model predictions and the DNS data will be addressed in the Discussion. The somewhat overestimated stabilization caused by the imposed axial rotation can therefore most likely be ascribed to the $\overline{u_z u_\theta}$ component.

The rms distributions of the axial and radial normal stress components are shown in Fig. 5. The model predictions compare reasonably well with the DNS data in the nonrotating case, whereas the turbulent energy level is significantly overpredicted in the pipe core at $N = 0.32$. This tendency is even more pronounced at higher rotation rates. Figure 6 displays the turbulent kinetic energy distribution at $Re = 2 \times 10^4$ and $N = 0$ and 0.5. In contrast to the experimental results,[6] which showed that the turbulent kinetic energy in the

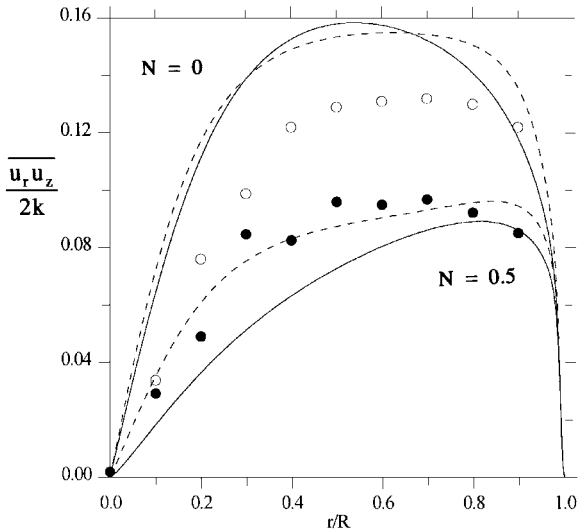


**Fig. 7 Structural parameter at $Re = 2 \times 10^4$: symbols, experiments[6]; ——, IP; - - - -, SSG; ○, $N = 0.0$; and ●, $N = 0.5$.**

rotating pipe fell below that in the stationary pipe, both the SSG and IP models predict an enhanced turbulence level with increased rotation. The same phenomenon was also observed by Shih et al.[8] Here, it should be recalled that the scaling of the turbulent kinetic energy does not influence the results in Fig. 6 because the Reynolds number based on the mean bulk velocity is the same in the predictions and in the experiments.

Finally, the substantial reduction of the structural parameter $\overline{u_r u_z}/2k$ in Fig. 7 with increased rotation is well captured, especially by the SSG model. These results confirm the findings of Yoo et al.,[2] namely, the existence of nonequilibrium turbulence in the logarithmic layer.

## Discussion

Frame indifference is an essential issue in the modeling of turbulent flows affected by centrifugal forces arising from streamline curvature or Coriolis forces due to system rotation. The convective transport $C_{ij}$ was included in the linear IP model for the rapid pressure–strain process for the sake of generality, although it was anticipated that its effect would be modest in the present case. Pettersson et al.[14] explored the influence of this particular term by means of an explicit ARSM closure. By neglecting viscous and turbulent diffusion, it was observed that the inclusion of $C_{ij}$ in the IP model reduced the effect of streamline curvature on the turbulence. Moreover, that standard IP model (without convective transport) differed only marginally from the modified model if the dimensionless curvature parameter $(U_\theta/r)/(\mathrm{d}U_\theta/\mathrm{d}r) > -0.1$. Very recently, Malin and Younis[10] compared predictions of axially rotating pipe flow with and without $C_{ij}$ included in the linear IP model in conjunction with a conventional SMC and observed that the inclusion of $C_{ij}$ led to only a modest improvement of the circumferential mean velocity.

It is noteworthy that both cubic models fail completely in the present study at the high Reynolds numbers and, furthermore, that the RLA model is unable to predict the rapidly rotating pipe flow even at low Reynolds numbers; cf. Table 2. This suggests that the reason for the failure should be sought in the pressure–strain models. Figures 8a and 8b display the leading terms in the budget of the important $\overline{u_r u_\theta}$ component at $N = 0.32$ for the SSG and FLT models, respectively. The magnitude of the relaxed pressure–strain tensor $(\wp_{r\theta})$ is significantly overpredicted by the FLT model in the logarithmic layer, whereas good agreement is obtained with the SSG model. Closer examination of the individual terms in the FLT pressure–strain model reveals that the major negative contribution comes from the quadratic term $(a^2_{ip}S_{pj} + a^2_{jp}S_{pi} - \frac{2}{3} < a^2 S > \delta_{ij})$, which has no counterpart in the SSG model. The cubic term, on the other hand, makes a positive contribution to $\wp_{r\theta}$. This suggests that the coefficients associated with these terms could be altered to make the model applicable also to higher rotation numbers. The importance of the cubic term for flows affected by centrifugal or Coriolis forces has been pointed out by Fu et al.[20] Because both models have the same tensorial basis, it seems, however, somewhat puzzling that the RLA model completely fails, whereas the FLT model produces reasonable results in the low-Reynolds-number case. This can most likely be attributed to the fact that the RLA model employs variable coefficients, whereas the FLT model uses fixed (constant) coefficients. It is, however, very difficult to analyze the direct effect of this difference due to the complexity of the models.

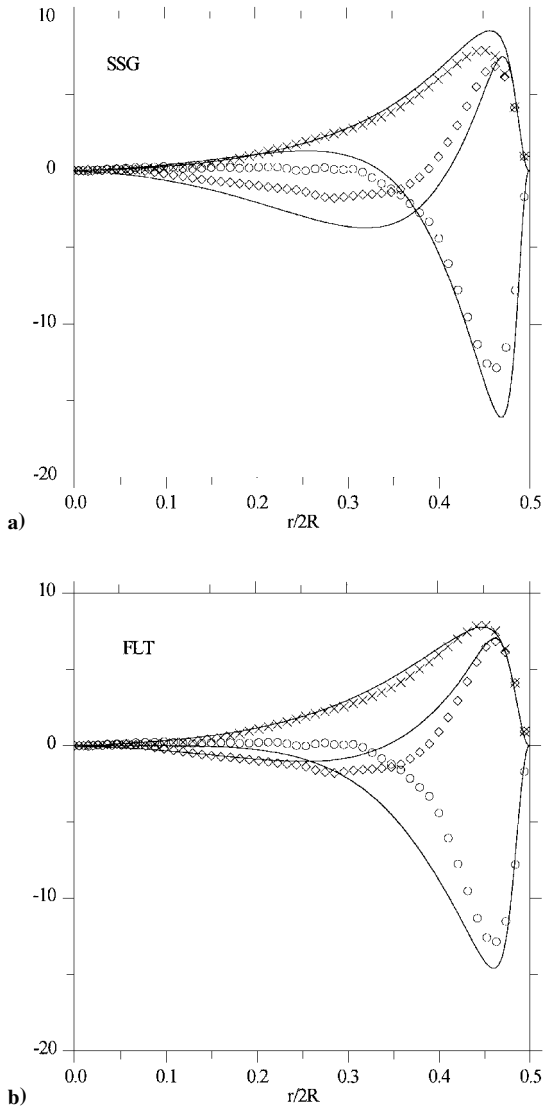


**Fig. 8 Leading terms in the $\overline{u_r u_\theta}$ budget at $Re_* = 3.6 \times 10^2$ and $N = 0.32$: symbols, DNS[16]; ×, $-C_{r\theta}$; ◇, $P_{r\theta}$; ○, $\wp_{r\theta}$, scaled by $u_*^3/2R$; and lines, model predictions.**

Consider instead the equilibrium solution of the $\overline{u_r u_\theta}$ transport equation, which can be written as

$$\frac{\overline{u_r u_\theta}}{k} = -\frac{\overline{u_r^2}}{\varepsilon}\frac{\mathrm{d}U_\theta}{\mathrm{d}r}\frac{1 - C_2}{C_1}\left(1 - \frac{2\alpha - 1}{n}\right) \tag{11}$$

where the IP model is used for simplicity. It is furthermore assumed that $\overline{u_\theta^2}/\overline{u_r^2} \approx \alpha$ and $U_\theta \propto r^n (\alpha, n > 0)$. The model constants take their standard values[12] $C_1 = 1.22$ and $C_2 = 0.6$. Because both DNS data and experimental results indicate that $n \approx 2$, $\overline{u_r u_\theta} > 0$ only if $\alpha \gtrsim \frac{3}{2}$. Hence the separation between the circumferential and radial normal stress components seems crucial to reproduce the observed distribution of the circumferential mean velocity because $U_\theta$ depends directly on the sign of $\overline{u_r u_\theta}$; cf. Eq. (10). It is interesting to note that the predicted $\alpha$ obtained with the FLT model is significantly larger than that returned by the RLA model in the nonrotating case. This behavior is an indirect consequence of the variable coefficients in the RLA model and provides a possible explanation of why the FLT model performs better than the RLA model. Note, however, that the results obtained with the RLA model in the nonrotating case are

in better agreement with the DNS data than the predictions obtained with any other pressure–strain model considered in this study.

Similarly, the equilibrium solution of the $\overline{u_z u_\theta}$ transport equation can be written as

$$\frac{\overline{u_z u_\theta}}{k} \approx -\frac{1 - C_2}{C_1} \frac{\overline{u_r u_z}}{\varepsilon} \frac{1}{r} \frac{\mathrm{d}}{\mathrm{d}r}(U_\theta r) \tag{12}$$

if the IP model is used and the assumption $\overline{u_r u_\theta} \ll \overline{u_r u_z}$ is invoked; cf. Fig. 4. It is thus clear from Eq. (12) that the model will return $\overline{u_z u_\theta} < 0$, as was indeed the case in Fig. 4c, if the model constants ($C_1$ and $C_2$) take their standard values. In addition, due to the underlying assumption of local equilibrium turbulence, the sign of the predicted $\overline{u_z u_\theta}$ component is solely attributed to the pressure–strain model. However, the sign of $\overline{u_z u_\theta}$ could be altered by taking $C_2 > 1$ or $C_1 < 0$ but not without serious implications. It is furthermore interesting that the flowfield in an axially rotating pipe resembles that of the core of a free swirling turbulent jet, i.e., the region in which $\mathrm{d}U_\theta/\mathrm{d}r > 0$. Younis et al.[21] conducted SMC computations with both linear and nonlinear pressure–strain models of this particular case. Interestingly enough, they reported that negative values of the $\overline{u_z u_\theta}$ component were predicted in the region close to the axis, i.e., opposite of that indicated by experimental results. It was observed, furthermore, that a pressure–strain model that retained nonlinear elements of the Reynolds-stress tensor (SSG) produced a lower level of $\overline{u_z u_\theta}$ than a linear model, i.e., fully in accordance with the present findings.

The preceding discussion makes it clear that the prediction of negative shear stress $\overline{u_z u_\theta}$ is a direct consequence of conventional modeling of the pressure–strain process, and even the sophisticated models used in the present study produce $\overline{u_z u_\theta} < 0$. It is particularly noteworthy that the model predictions are consistent with the measurements by Kikuyama et al.[1] and Imao et al.[6] in this respect, whereas recent DNSs due to Eggels et al.[16] and Orlandi and Fatica[22] show the opposite, namely, that $\overline{u_z u_\theta}$ is basically positive and exhibits a distinct peak near the wall; cf. Fig. 4c. The substantial covariance between $u_z$ and $u_\theta$ is most likely associated with the helical pattern of the streamlines,[16] which results in tilting of the coherent structures in the near-wall region. Eggels et al.[16] examined the $\overline{u_z u_\theta}$ budget and found that generation of $\overline{u_z u_\theta}$ occurs via pressure–strain processes, whereas production and convection terms are loss terms. Thus, the pressure–strain term has the same sign as the shear stress itself, thereby suggesting that the commonly used return-to-isotropy model needs to be overcome by other model elements. Within the framework of SMC modeling, the sign of $\overline{u_z u_\theta}$ is essential because this shear stress component indirectly affects the axial mean velocity $U_z$ via the $\overline{u_r u_z}$ equation. Therefore, the contradictory findings in the laboratory investigations[1,6] ($\overline{u_z u_\theta} < 0$) and in the numerical experiments[16,22] ($\overline{u_z u_\theta} > 0$) need to be sorted out to assist any further progress in the modeling of axially rotating pipe flow.

## Conclusion

The present study has shown that the novel wall treatment by means of elliptic relaxation seems capable of capturing the important near-wall effects in an axially rotating pipe flow—a flow that imposes a challenging test for any turbulence closure. The elliptic relaxation approach accounts for near-wall effects via the solution of a linear equation, which can be used in conjunction with any quasihomogeneous pressure–strain model, and thus avoids highly nonlinear damping functions. The modeling of the pressure–strain process is of crucial importance within the framework of Reynolds stress transport modeling. It has been shown that a pressure–strain model that retains terms quadratic in the Reynolds stresses, like the SSG model, is most suitable to faithfully reproduce most of the effects observed in axially rotating pipe flow. Highly nonlinear (cubic) pressure–strain models, on the other hand, fail severely in the present case. It is finally noteworthy that the particular gradient-diffusion model adopted in the closure model seems to have only minor influence on the results.

## Acknowledgments

The work reported here was accomplished while the first author was a doctoral student at the Norwegian University of Science and Technology, Division of Applied Mechanics. The authors are grateful to F. T. M. Nieuwstadt and J. G. M. Eggels for kindly providing us with the (unpublished) direct numerical simulation results of the axially rotating pipe flow. The referees are acknowledged for their constructive comments, which helped to improve the final version of the paper. This paper is a slightly expanded and revised version of a paper presented at the 11th Symposium on Turbulent Shear Flows, Grenoble, France, Sept. 8–10, 1997.

## References

[1] Kikuyama, K., Murakami, M., and Nishibori, K., "Development of Three-Dimensional Turbulent Boundary Layer in an Axially Rotating Pipe," *Journal of Fluids Engineering*, Vol. 105, June 1983, pp. 154–160.

[2] Yoo, G. J., So, R. M. C., and Hwang, B. C., "Calculation of Developing Turbulent Flows in a Rotating Pipe," *Journal of Turbomachinery*, Vol. 113, Jan. 1991, pp. 34–41.

[3] Murakami, M., and Kikuyama, K., "Turbulent Flow in Axially Rotating Pipes," *Journal of Fluids Engineering*, Vol. 102, March 1980, pp. 97–103.

[4] Kikuyama, K., Murakami, M., Nishibori, K., and Maeda, K., "Flow in an Axially Rotating Pipe (A Calculation of Flow in the Saturated Region)," *Bulletin of the Japan Society of Mechanical Engineers*, Vol. 26, No. 214, 1983, pp. 506–513.

[5] Reich, G., and Beer, H., "Fluid Flow and Heat Transfer in an Axially Rotating Pipe—I. Effect of Rotation on Turbulent Pipe Flow," *International Journal of Heat and Mass Transfer*, Vol. 32, No. 3, 1989, pp. 551–561.

[6] Imao, S., Itoh, M., and Harada, T., "Turbulent Characteristics of the Flow in an Axially Rotating Pipe," *International Journal of Heat and Fluid Flow*, Vol. 17, No. 5, 1996, pp. 444–451.

[7] Hirai, S., Takagi, T., and Matsumoto, M., "Predictions of the Laminarization Phenomena in an Axially Rotating Pipe Flow," *Journal of Fluids Engineering*, Vol. 110, Dec. 1988, pp. 424–430.

[8] Shih, T.-H., Zhu, J., Liou, W. W., Chen, K.-H., Liu, N.-S., and Lumley, J. L., "Modeling of Turbulent Swirling Flows," *Proceedings of the 11th Symposium on Turbulent Shear Flows*, Institut National Polytechnique de Grenoble, Université Joseph Fourier, Grenoble, France, 1997, pp. 31.1–31.6.

[9] Wallin, S., and Johansson, A. V., "A New Explicit Algebraic Reynolds Stress Turbulence Model for 3D Flow," *Proceedings of the 11th Symposium on Turbulent Shear Flows*, Institut National Polytechnique de Grenoble, Université Joseph Fourier, Grenoble, France, 1997, pp. 13.13–13.17.

[10] Malin, M. R., and Younis, B. A., "The Prediction of Turbulent Transport in an Axially Rotating Pipe," *International Communications in Heat and Mass Transfer*, Vol. 24, No. 1, 1997, pp. 89–98.

[11] Speziale, C. G., Younis, B. A., and Berger, S. A., "Analysis and Modeling of Turbulent Flow in an Axially Rotating Pipe," Dept. of Aerospace and Mechanical Engineering, TR AM-97-031, Boston Univ., Boston, MA, Nov. 1997.

[12] Durbin, P. A., "A Reynolds-Stress Model for Near-Wall Turbulence," *Journal of Fluid Mechanics*, Vol. 249, 1993, pp. 465–498.

[13] Pettersson, B. A., and Andersson, H. I., "Near-Wall Reynolds-Stress Modelling in Noninertial Frames of Reference," *Fluid Dynamics Research*, Vol. 19, No. 5, 1997, pp. 251–276.

[14] Pettersson, B. A., Andersson, H. I., and Hjelm-Larsen, Ø., "Analysis of Near-Wall Second-Moment Closures Applied to Flows Affected by Streamline Curvature," *Engineering Turbulence Modelling and Experiments 3*, edited by W. Rodi and G. Bergeles, Elsevier, Amsterdam, The Netherlands, 1996, pp. 49–58.

[15] Eggels, J. G. M., Unger, F., Weiss, M. H., Westerweel, J., Adrian, R. J., Friedrich, R., and Nieuwstadt, F. T. M., "Fully Developed Turbulent Pipe Flow: A Comparison Between Direct Numerical Simulation and Experiment," *Journal of Fluid Mechanics*, Vol. 268, 1994, pp. 175–209.

[16] Eggels, J. G. M., Boersma, B. J., and Nieuwstadt, F. T. M., "Direct and Large-Eddy Simulations of Turbulent Flow in an Axially Rotating Pipe," Lab. for Aero- and Hydrodynamics, Delft Univ. of Technology, Delft, The Netherlands, Oct. 1994.

[17] Fu, S., "Modelling of the Pressure-Velocity Correlation in Turbulence Diffusion," *Computers and Fluids Journal*, Vol. 22, No. 2/3, 1993, pp. 199–205.

[18] Speziale, C. G., Sarkar, S., and Gatski, T. B., "Modelling the Pressure-Strain Correlation of Turbulence: An Invariant Dynamical Systems Approach," *Journal of Fluid Mechanics*, Vol. 227, 1991, pp. 245–272.

[19] Ristorcelli, J. R., Lumley, J. L., and Abid, R., "A Rapid-Pressure Covariance Representation Consistent with the Taylor-Proudman Theorem Materially Frame Indifferent in the Two-Dimensional Limit," *Journal of Fluid Mechanics*, Vol. 292, 1995, pp. 111–152.

[20] Fu, S., Launder, B. E., and Tselepidakis, D. P., "Accommodating the Effects of High Strain Rates in Modelling the Pressure–Strain Correlation," Mechanical Engineering Dept., Univ. of Manchester Inst. of Science and Technology, TR TFD/87/5, Manchester, England, UK, March 1987.

[21] Younis, B. A., Gatski, T. B., and Speziale, C. G., "Assessment of the SSG Pressure–Strain Model in Free Turbulent Jets with and Without Swirl," *Journal of Fluids Engineering*, Vol. 118, Dec. 1996, pp. 800–809.

[22] Orlandi, P., and Fatica, M., "Direct Simulations of Turbulent Flow in a Pipe Rotating About Its Axis," *Journal of Fluid Mechanics*, Vol. 343, 1997, pp. 43–72.

C. G. Speziale
*Associate Editor*